Late-stage coarsening of an unstable structured liquid film

Ratchana Limary and Peter F. Green
Texas Materials Institute and Department of Chemical Engineering, The University of Texas at Austin, Austin, Texas 78712
(Received 21 February 2002; revised manuscript received 28 May 2002; published 8 August 2002)

Thin films of poly(styrene-*b*-methyl methacrylate) diblock copolymers *above* the bulk order-disorder transition temperature, within a certain thickness range, are structurally unstable on SiO_x/Si substrates. They dewet autophobically, forming droplets on a self-assembled brush. We investigated the late-stage evolution, coarsening, of the droplets on the brush. The average droplet cross-sectional area $\langle S\rangle$ increased with time, $\langle S\rangle \propto t^{\gamma}$. This was accompanied by a decrease in the number of droplets per unit area with time, $N(t)\propto t^{-\gamma}$. We analyzed the droplet size distribution, $F(S/\langle S\rangle)$ vs $S/\langle S\rangle$, and found that the shape of the curve was virtually identical at different stages throughout the process. This suggests that a structural self-similarity is associated with the process. A comparison of $F(S/\langle S\rangle)$ vs $S/\langle S\rangle$ data with distributions based on Ostwald ripening and coalescence cluster coarsening (dynamic and static) mechanisms strongly indicates that the dominant coarsening mechanism involved motion of droplets across the brush and subsequent coalescence, i.e., dynamic coalescence coarsening, not Ostwald ripening.

DOI: 10.1103/PhysRevE.66.021601 PACS number(s): 68.08.−p

I. INTRODUCTION

Coarsening mechanisms are responsible for the late-stage time-dependent evolution of the morphology of a variety of bulk and thin film systems [1]. In bulk *A-B* mixtures that undergo phase separation via a spinodal decomposition mechanism or otherwise, coarsening mechanisms are responsible for the time-dependent late-stage growth and shape of *A*-rich and *B*-rich phases that characterize the microstructure of the material. When thin films become structurally unstable and dewet an underlying substrate, subsequently forming droplets, coarsening also accounts for the time-dependent evolution of the shape and size and number of droplets [2]. In thinly deposited layers of metals on substrates, depending on the conditions, thickness, temperature, deposition rate, and the substrate, different coarsening mechanisms or a combination of mechanisms, contribute to the growth of the layers [1,3].

Mechanisms of coarsening include, (1) Ostwald ripening [4–11] and (2) coalescence, dynamic and static coalescence [1,3,8,12–17]. In *Ostwald ripening*, mass is transferred between stationary clusters of atoms or molecules when atoms detach/evaporate from one cluster and diffuse/condense onto another cluster in the vicinity. *Dynamic coalescence* involves diffusion and subsequent merging of clusters. *Static coalescence* occurs due to a fluctuation in the shape of a cluster whose center of mass is stationary. This fluctuation leads to contact and subsequent merging of nearby clusters.

We are interested in the late-stage structural evolution of *A-B* diblock copolymer thin films that become unstable, dewet autophobically, forming droplets on an underlying copolymer brush (substrate) layer. This is illustrated in Fig. 1. With this in mind, we begin with brief comments regarding block copolymer thin films. Below an order-disorder transition (ODT), *A-B* diblock copolymer films form nanoscale structures of a variety of symmetries (spheres, lamellar, cylinders), depending on the relative volume fractions, *f*, of the *A* and *B* components comprising the chain. The ODT is determined by the total number of segments on the chain, *N*, and the Flory-Huggins (energetic) interaction parameter, χ [18]. For example, alternating *A-B-A-B* lamellae comprise the structure of bulk symmetric ($f=\frac{1}{2}$) diblock copolymers when $\chi N>10.5$. On the other hand, the bulk structure is isotropic when $\chi N<10.5$.

In thin films, either the *A* or *B* component will exhibit a preferential affinity for the substrate, except in the case of a neutral surface, and for the free surface. The interfacial free energy per unit area, ΔF, is a periodic function of the film thickness, *h*. Regions of film thickness where the curvature is negative, $\partial^2\Delta F/\partial h^2<0$, are unstable toward the growth of capillary wave instabilities [19]. If the copolymer film is below the bulk ODT, surface relief structures, islands, holes, or interconnected structures, of height equal to the interlamellar

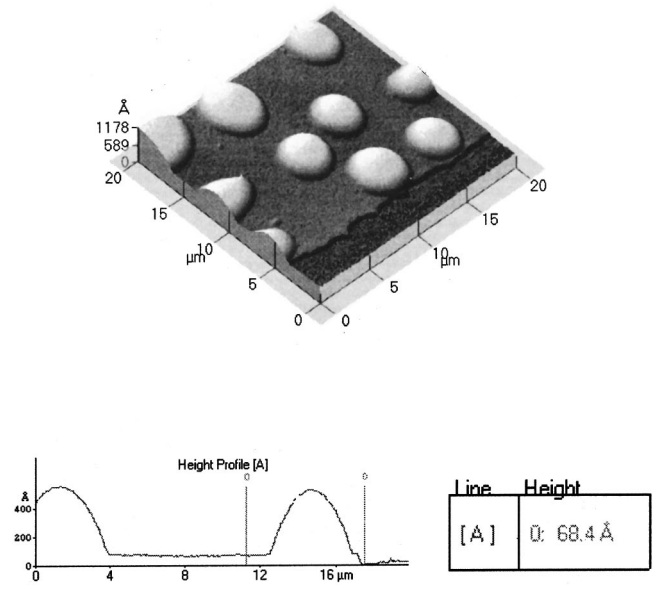

FIG. 1. Shown here is a typical AFM image of a PS-*b*-PMMA sample ($\chi N<10.5$, $f=\frac{1}{2}$) that autophobically dewets a SIO_x/Si substrate. Droplets form on a self-assembled brush layer of thickness 7 nm.

spacing, L, develop at the free surface if the film thickness does not meet certain criteria. In symmetric diblock copolymer films, for example, the topographies develop if the film thickness $h \neq (n+\frac{1}{2})L$ [20–24]. On the other hand, if the film thickness $h=(n+\frac{1}{2})L$, then the surface relief structures are absent and the surface is smooth. The late-stage coarsening of the islands and holes has been shown to be governed by a power-law exponent, suggestive of an Ostwald ripening mechanism where transport is diffusion controlled [25,26]. Growth of the interconnected structures in films on patterned surfaces appears to be governed by a larger power-law exponent, between $\frac{1}{2}$ and 1 [27].

In this paper we examine the late-stage coarsening dynamics of droplets that result from the dewetting of a polystyrene-*b*-poly(methyl methacrylate) (PS-*b*-PMMA) thin film of thickness $h=11.5$ nm ($\chi N=7.5$ and $f=0.5$) on a SiO_x/Si substrate. Films, in the thickness range $L/2<h<5L/2$ ($L=14$ nm), become unstable and dewet autophobically [2,21,28,29]. Specifically, droplets reside on a brush layer of thickness $L/2$ on the SiO_x/Si substrate. This layer, as discussed elsewhere, is due to ordering (structuring) induced into this copolymer by the SiO_x/Si substrate [21,28]. We show that the late-stage coarsening dynamics of these droplets on the substrate, or brush layer (Fig. 1), are governed primarily by a dynamic coalescence process, not Ostwald ripening.

II. EXPERIMENT

A PS-*b*-PMMA diblock copolymer film of thickness $h=11.5$ nm was prepared on a SiO_x/Si substrate using photoresist spinner. Toluene was used as a solvent to dissolve this polymer whose total molecular weight was $M=20\,500$ ($M_{PS}=9800$ and $M_{PMMA}=10\,700$) and polydispersity index $M_w/M_n=1.14$. The polymer was purchased from Polysciences, Inc. Samples were annealed at 170 °C for varying periods of time under vacuum. Atomic force microscopy (AFM) topographic analyses were performed on the sample quenched to room temperature at specific intervals during the process.

Figure 2 shows AFM images at three different stages of evolution, 215, 405, and 7345 min. The coarsening is evident in parts (c) and (b). The AFM images (256×256 pixels) were converted to black and white pixels for image analyses. The images were threshold such that black was assigned to the substrate and white to the droplets. The following information was determined from each image using Clemex Vision image analysis software v2.2 (Clemex Technologies, Inc.). The fractional surface area covered by droplets, $\phi(t)$, the average surface area per droplet, $\langle S(t)\rangle$, and the number of droplets per unit area, $N(t)$, were determined at various stages during the coarsening of each film. In addition, a shape factor, S_f, was determined for the droplets in all the images. The shape factor is defined such that $S_f=4\pi A/P$, where A is the cross-sectional area of a droplet and P is its perimeter. We will later use the information from these images to compare the applicability of coarsening models to learn about the mechanism of coarsening.

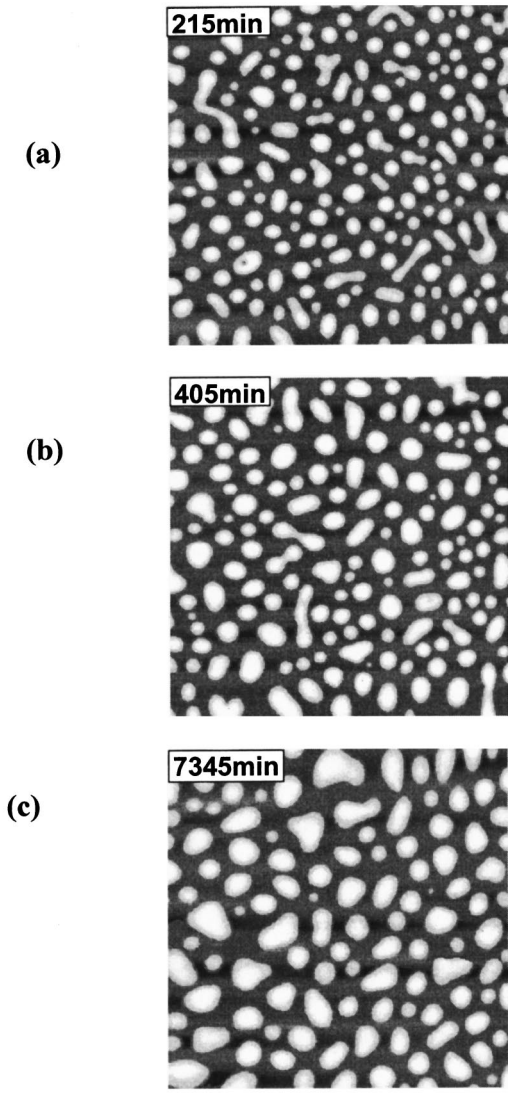

FIG. 2. The evolution of topography of the sample is shown here at three different times during coarsening. The average droplet size increases with time.

III. RESULTS

The fractional surface area covered by polymer, $\phi(t)$, initially decreases with time before reaching a constant value, as shown in Fig. 3(a). The time at which $\phi(t)$ becomes independent of time, $t_\phi=200$ min, denotes the onset of the formation of droplets on the substrate. Note that the data in Fig. 2 were obtained for $t>t_\phi$. The average shape factor, or roundness factor, S_f, provides a measure of the relative circularity of planar shapes of the droplets ($S_f=1$ for a circle). $S_f(t)$ increases with time before approaching a constant value at later times [Fig. 3(b)]. This transition, where the average shape factor becomes approximately constant, occurs when the polymer surface coverage $\phi(t)$ becomes constant (i.e., $t=t_\phi$). We further note that when $t>t_\phi$ the

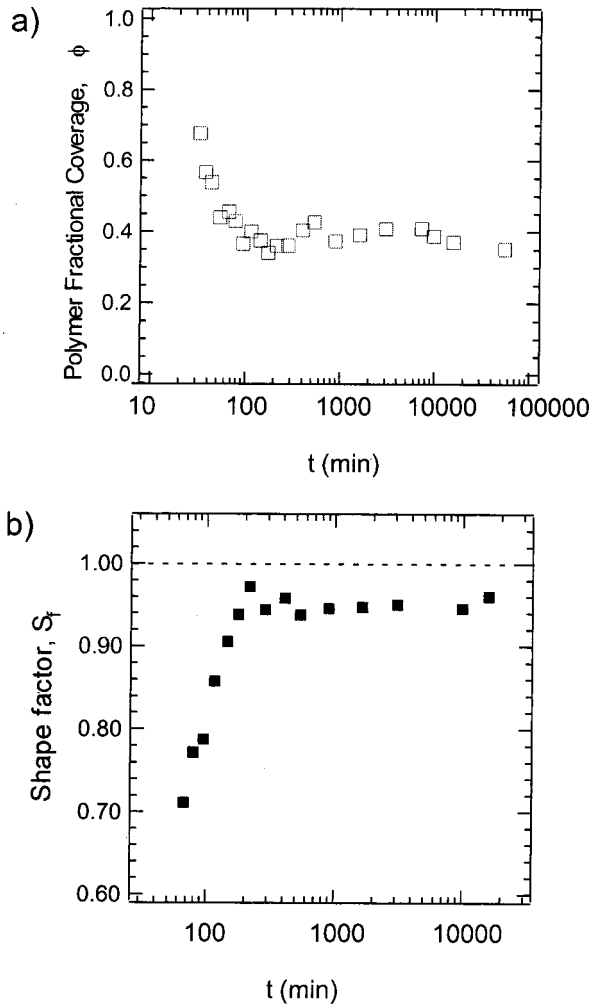

FIG. 3. The time dependences of the fractional coverage, $\phi(t)$, and of the shape factor, $S_f(t)$, are shown here.

height of the droplets is approximately constant. Moreover, the angle of contact of the droplets on the brush is very small, $\theta = 1°$. This small value of θ has important implications regarding the coarsening mechanism in this system.

The average projected, planar, surface area, $\langle S(t)\rangle$, exhibits a power-law dependence on time,

$$\langle S(t)\rangle \propto t^{\gamma}. \tag{1}$$

This is accompanied by a decrease in the number of droplets with time,

$$N(t) \propto t^{-\gamma}. \tag{2}$$

The magnitude of the exponent γ is comparable for $N(t)$ and $\langle S(t)\rangle$, as one would expect if the mass is conserved and the height of the droplets is constant. The value of the power-law exponent from both sets of data in Fig. 4 is $\gamma = 0.18 \pm 0.005$. That the magnitude of the power-law exponent is much less than $\frac{2}{3}$ suggests that coarsening might not be entirely capillarity driven. This may not be surprising considering that the angle of contact is very small. Knowledge of the power-law exponent alone is not conclusive [8]. We need

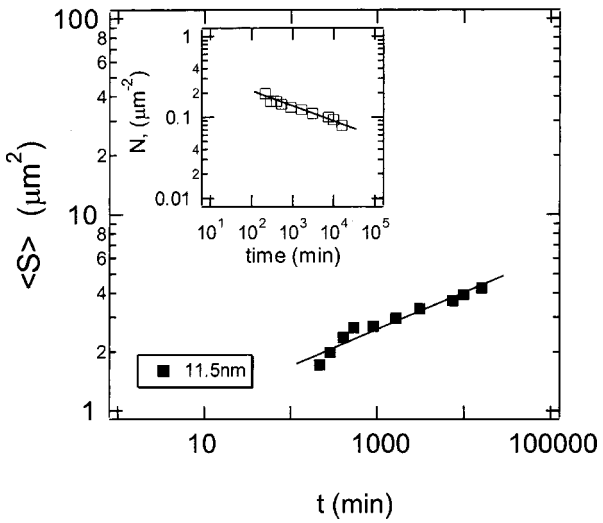

FIG. 4. The increase average area per droplet, $\langle S\rangle$, with time is described by a power law, $\langle S(t)\rangle \sim t^{2/5}$. The increase in $\langle S\rangle$ is accompanied by a decrease in $N(t)$, where $N(t) \sim t^{-2/5}$, as expected.

to examine the process in further detail before any definitive statements can be made regarding possible coarsening mechanisms. We will do two things. (1) We will first determine the probability distribution describing the droplet sizes and compare them with predictions based on different coarsening mechanisms. (2) Secondly, we will examine ''snapshots'' of the process at different times to identify specific processes.

IV. DISCUSSION

A. Coarsening models

1. Ostwald ripening

Several models have been used to describe cluster growth on surfaces and in other environments. Ostwald ripening is limited to systems with low coverage. The clusters are considered fixed spatially and exchange of mass occurs via atoms (molecules) detaching from the cluster and diffusing across the surface of the substrate from small clusters to large clusters [4–7,9–11]. Large clusters increase in size at the expense of small ones thereby reducing the total surface to volume ratio (or the interfacial energy) of the system. The chemical potential of a cluster is proportional to its radius of curvature, thus large clusters grow while small clusters dissolve. According to this model, there is a critical cluster size that determines whether a cluster grows or shrinks.

The average cluster size $\langle S\rangle$ is predicted to increase with time such that $\langle S(t)\rangle^{1/2} \sim \langle R(t)\rangle \sim t^{\beta/2}$. The value of β depends on whether the rate limiting step for transport is associated with detachment (evaporation-condensation) of atoms ($\beta = 1$) or by surface diffusion ($\beta = 2/3$). The cluster size distribution function $F(S,t)$ is a normalized probability distribution that defines the number of clusters of each size in a fixed area as a function of time. At long times, $F(S')$ is independent of t, having a scale invariant asymptotic form $F(S,t) = F(S')$, where $S' = S/\langle S\rangle$ is a dimensionless size. For two-dimensional (2D) clusters on a 2D surface, $F(S')$ is

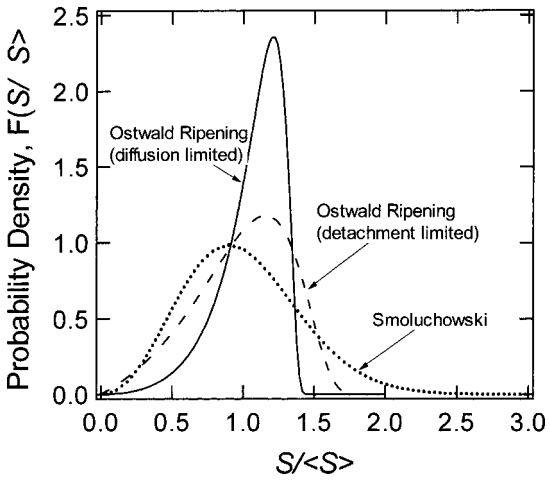

FIG. 5. Theoretical probability density distribution functions, $F(S/\langle S\rangle)$ versus $S/\langle S\rangle$, are shown here for coalescence and Ostwald ripening models.

given by the following equation when the rate limiting step is diffusion of species, and $S'<3/2$:

$$F(S')=\frac{CS'^{2}\exp\left(\frac{-1}{\frac{3}{2}-S'}\right)}{(\frac{3}{2}-S')^{28/9}(3+S')^{17/9}}. \tag{3}$$

Otherwise $F(S')=0$ for $S'>0$ [8]. C is a normalization constant. When the rate determining step is the detachment of the atoms from the clusters, $F(S')$ is given by the following equation if $S'<2$:

$$F(S')=\frac{S'}{2}\left(\frac{2}{2-S'}\right)^{4}\exp\left(\frac{-2S'}{2-S'}\right), \tag{4}$$

otherwise when $S'>2$, $F(S')=0$.

The shape of the cluster size distribution, $F(S/\langle S\rangle)$ vs $S/\langle S\rangle$, associated with coarsening due to an Ostwald ripening process is shown in Fig. 5. Note that this function is a negatively skewed cure; it is steep at large $S/\langle S\rangle$ and has a tail extending to zero as $S/\langle S\rangle$ approaches 0. The cluster size $S/\langle S\rangle$ at which the function is a maximum is the critical cluster size below which clusters are unstable and shrink in size.

2. Coalescence models

In dynamic coalescence (cluster diffusion), clusters of all sizes are mobile and growth occurs when clusters collide and coalesce to increase the mean cluster size. This coarsening process is often described using the Smoluchowski equation, which is a mean field rate equation that describes the change in cluster density in which the collisions are assumed to be binary in nature [3,12,14]. In this model, the atoms at the vapor interface of the cluster undergo random Brownian motion to change the position of the cluster center of mass. The dependence of $\langle S\rangle$ on t is determined by the cluster diffusion coefficient. The cluster diffusion coefficient depends on the size of the clusters (small clusters are more mobile than large clusters) and on effective interactions between the clusters. Coarsening due to coalescence from cluster diffusion is characterized by a unique *time invariant* cluster size distribution function $F(S'=S/\langle S\rangle)$. The distribution function is different from those of Ostwald ripening [cf. Eqs. (3) and (4)]. If the kinetics are modeled using the Smoluchowski equation, assuming binary collisions, the size distribution function describing the cluster diffusion mechanism can be expressed as

$$F(S')=\frac{dW(WS')^{d(\alpha+1-1/d)}}{\Gamma(\alpha+1)}\exp(-WS')^{d}. \tag{5}$$

In this equation, d is the spatial dimension of the system ($d=2$ for flat clusters on a surface) and $W=\Gamma(\alpha+1+1/d)/\Gamma(\alpha+1)$, where Γ is the gamma function. The value of α provides information about the mechanism of coarsening. If the diffusion coefficient exhibits power-law scaling, $D_S\propto n^{-\alpha}$, where n is the number of molecules per cluster. The mean cluster size scales as $\langle S\rangle\sim t^{\gamma}$ where the exponent $\gamma=\delta/2$ and $\delta=1/d(\alpha+1)$. For peripheral diffusion, where the periphery of the droplet fluctuates in order to facilitate motion, $\alpha=\frac{3}{2}$. For terrace diffusion, where species are evaporated from the cluster and their motion is limited by diffusion, $\alpha=1$. For motion facilitated by evaporation condensation of species from the peripheral regions of a cluster, $\alpha=\frac{1}{2}$.

Log-normal shaped cluster size distributions, such as the dynamic Smoluchowski coalescence equation (Fig. 5), are associated with systems where growth is dominated by liquidlike coalescence. Such distributions are positively skewed curves, with the longer tail extending toward larger cluster sizes. This is due to the fact that the diffusivity of a cluster is size dependent. The large clusters are less mobile than the small clusters and the distribution function exhibits a tail that extends towards larger cluster sizes.

B. Comparison of coarsening models

The probability distribution of droplet sizes was determined for each AFM micrograph from the values of the two-dimensional projected surface area S of each droplet in the image. For example, Fig. 6 shows a plot of the droplet size probability distribution at various times of annealing. The probability distribution broadens with time. Moreover, a shift toward larger values of S occurs, indicating coarsening of the droplets. This can be explained by considering that early in the coarsening process the polymer droplets exhibit a relatively small size distribution. However, as coarsening proceeds the breadth of the distribution broadens, indicating that the droplets become less uniform in size with time during this stage. This is due to differences in diffusivity of the different sized droplets.

The droplet size probability distributions at each time ($t>t_{\phi}$) is normalized and the function $F(S/\langle S\rangle)$ is plotted vs $S/\langle S\rangle$ (Fig. 7). The distribution is independent of time and collapses onto one curve. The tail of this curve extends toward large droplet sizes in the normalized probability distri-

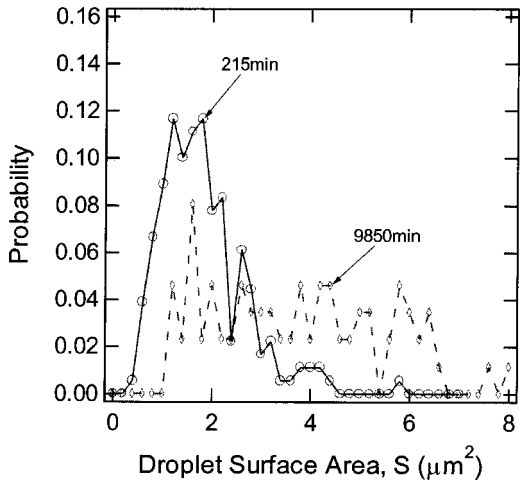

FIG. 6. The size distributions (non-normalized) are shown here for two different times for droplets from the sample.

bution $F(S/\langle S\rangle)$. This is consistent with dynamic coalescence and is due to the fact that large droplets are less mobile than small droplets. This is discussed further below.

In Fig. 8, the experimental droplet size distributions are compared to the predictions in order to gain further insight into the late-stage droplet evolution of the samples. The data points in this figure are averages of the data from Fig. 7 at the relevant times. These data show best agreement with the dynamic Smoluchowski coalescence equation, Eq. (5). The calculated *R*-squared error $R^2=0.96$ between the data and the Smoluchowski coalescence function using parameter $\alpha \approx 0.3\pm 0.1$, indicating that $\gamma=0.190\pm 0.015$. Clearly, the evolution and shape of the distribution function is consistent with the coalescence coarsening model and suggests a mechanism associated with the diffusivity of the individual droplets. The exponent obtained from fitting this distribution is comparable to that determined from measurements of the average area, $\langle S\rangle \sim t^{0.18}$ in Fig. 4. Clearly, the value of the exponent in Fig. 4 strongly indicates the absence of a capillarity driven process.

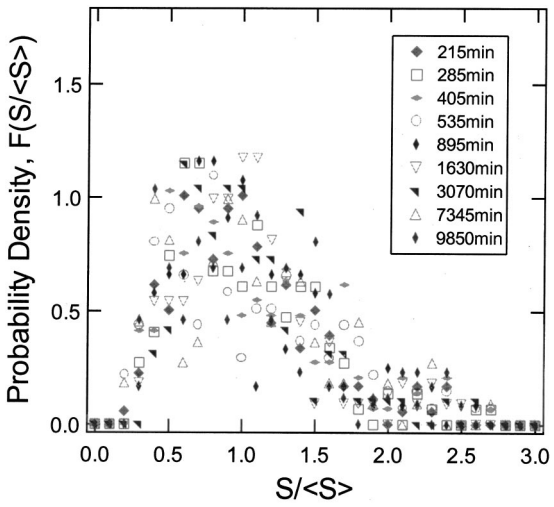

FIG. 7. Probability (normalized) density distribution functions are shown here at different times.

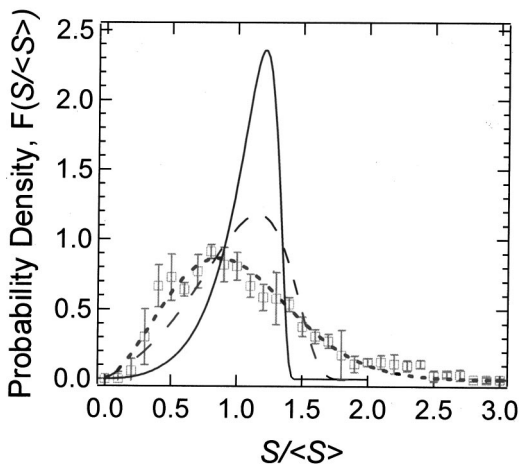

FIG. 8. The theoretical and experimental distributions are compared.

That γ lies between $\frac{1}{5}$ and $\frac{1}{6}$ raises an important issue regarding the mechanism of transport. A value of $\frac{1}{5}$ might not be completely justified in two dimensions but would be in three dimensions using $\alpha=1$, assuming that the theories are completely applicable to our system. With this in mind, it is worth noting that our system is not a true two-dimensional system. The coalescence model described here assumes that the system is flat, truly two dimensional, and that coalescence occurs via binary collisions. Our system involves droplets [$\phi(t)$ is nevertheless relatively constant in the regime of our experiments, $\langle S\rangle(t)N(t)\approx$const, and the angle of contact is small] and the latter assumption involving binary collisions is not necessarily always valid in our case. Hence it is not clear at this point how much one might rely on the precise value of the exponents in order to dictate the mechanism of transport. A study involving films of varying thicknesses would provide further insight into this issue. Nevertheless our main conclusion that coalescence instead of Ostwald ripening is the dominant mechanism for coarsening is confirmed.

Finally, while the *dynamic coarsening* mechanism is the dominant mechanism, other mechanisms are operative, though to a comparably lesser extent. First, dynamic and

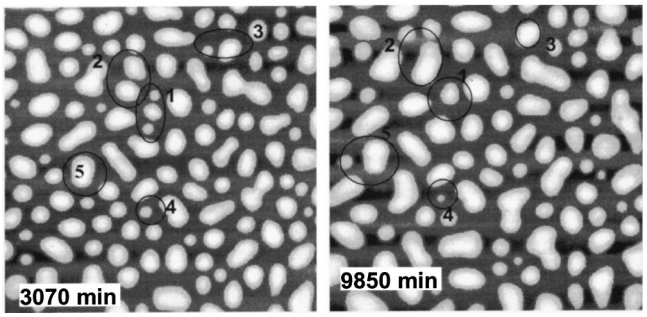

FIG. 9. Regions of the sample where coalescence and Ostwald ripening mechanisms occur are identified in this sample. Regions 1, 2, 3, and 4 illustrate coalescence whereas region 5 is consistent with Ostwald ripening. Ostwald ripening has a minor contribution.

static coalescence coarsening processes are operative. Shown in Fig. 9 are two images of droplets at times $t=3070$ (a) and 9850 min (b). The region identified as 1 contains three droplets at 3070 min. Later ($t=9850$ min) they merged to form one droplet. This would be an example of dynamic coalescence. In region 2 two droplets merged to form a larger one. This could have occurred via a static coalescence process, with the perimeters fluctuating and touching without either cluster moving its center of mass. An Ostwald ripening process is also evident in region 4, where the droplet became smaller with time, with its center of mass remaining stationary. This mechanism obviously plays a minor role. Based on our analysis of the images, the coalescence mechanism is indeed the dominant coarsening mechanism.

V. CONCLUSIONS

We examined the late-stage evolution of PS-*b*-PMMA droplets on a PS-*b*-PMMA brush. During this late stage, coarsening of the droplets occurred, wherein the average droplet size increased with time, $\langle S\rangle \propto t^{\gamma}$, accompanied by a decrease in the number of droplets per unit area with time, $N(t)\propto t^{-\gamma}$. We analyzed the droplet size distribution, $F(S/\langle S\rangle)$ vs $S/\langle S\rangle$, and found that the shape of the curve was virtually identical at different times throughout the coarsening process, suggesting a structural self-similarity of the process. These data were compared with Ostwald ripening and coalescence cluster coarsening models. The dynamic Smoluchowski coalescence distribution function $F(S/\langle S\rangle)$ showed best agreement with our data.

[1] M. Zinke-Allmang, Thin Solid Films **346**, 1 (1999).
[2] J.-L. Masson, R. Limary, and P. F. Green, J. Chem. Phys. **114**, 24 (2001).
[3] D. S. Sholl and R. T. Skodje, Physica A **231**, 631 (1996).
[4] P. W. Voorhees and M. E. Glicksman, Acta Metall. **32**, 2013 (1984).
[5] P. W. Voorhees, Annu. Rev. Mater. Sci. **22**, 197 (1992).
[6] K. Shorlin, S. Krylov, and M. Zinke-Allmang, Physica A **261**, 248 (1998).
[7] A. J. Ardell, Phys. Rev. B **41**, 2554 (1990).
[8] A. Lo and R. T. Skodje, J. Chem. Phys. **112**, 1966 (2000).
[9] B. K. Chakraverty, J. Phys. Chem. Solids **28**, 2401 (1967).
[10] B. K. Chakraverty, J. Phys. Chem. Solids **28**, 2413 (1967).
[11] A. J. Ardell, J. Eur. Ceram. Soc. **19**, 2217 (1999).
[12] M. Villarica, M. J. Casey, J. Goodisman, and J. Chaiken, J. Chem. Phys. **88**, 4610 (1993).
[13] D. J. Semin, A. Lo, S. E. Roark, R. T. Skodje, and K. L. Rowlen, J. Chem. Phys. **105**, 5542 (1996).
[14] J. Chaiken and J. Goodisman, Thin Solid Films **260**, 243 (1995).
[15] G. Rosenfeld, K. Morgenstern, M. Esser, and G. Comsa, Appl. Phys. A: Mater. Sci. Process. **A69**, 489 (1999).
[16] K. Masek, V. Matolin, and M. Gillet, Thin Solid Films **260**, 252 (1995).
[17] G. R. Carlow, Physica A **239**, 65 (1997).
[18] I. W. Hamley, *The Physics of Block Copolymers* (Oxford University Press, Oxford, 1998).
[19] K. R. Shull, Macromolecules **25**, 2122 (1992).
[20] G. Coulon, B. Collin, D. Ausserre, D. Chatenay, and T. P. Russell, J. Phys. (France) **51**, 2801 (1990).
[21] P. F. Green and R. Limary, Adv. Colloid Interface Sci. **94**, 53 (2001).
[22] A. P. Smith, J. F. Douglas, J. C. Meredith, E. J. Amis, and A. Karim, J. Polym. Sci., Part B: Polym. Phys. **39**, 2141 (2001).
[23] K. A. Orso and P. F. Green, Macromolecules **32**, 1087 (1999).
[24] T. P. Russell, Curr. Opin. Colloid Interface Sci. **1**, 107 (1996).
[25] P. Bassereau, D. Brodbreck, T. P. Russell, H. R. Brown, and K. R. Shull, Phys. Rev. Lett. **71**, 1716 (1993).
[26] A. J. Ardell, Phys. Rev. Lett. **74**, 4960 (1995).
[27] J. Heier, E. Sivaniah, and E. J. Kramer, Macromolecules **32**, 9007 (1999).
[28] R. Limary and P. F. Green, Macromolecules **32**, 8167 (1999).
[29] R. Limary and P. F. Green, Langmuir **15**, 5617 (1999).